Absence of telomerase and shortened telomeres have minimal effects on skin and pancreatic carcinogenesis elicited by viral oncogenes

David Argilla,[1,5,7] Koei Chin,[2,5] Mallika Singh,[1,6,8] J. Graeme Hodgson,[2,6,10] Marcus Bosenberg,[3,6,9] Carlos Ortiz de Solórzano,[4] Stephen Lockett,[4,11] Ronald A. DePinho,[3] Joe Gray,[2,4] and Douglas Hanahan[1,*]

[1]Department of Biochemistry and Biophysics, Diabetes Center, and Comprehensive Cancer Center
[2]Comprehensive Cancer Center and Department of Laboratory Medicine
University of California, San Francisco, San Francisco, California 94143
[3]Department of Medical Oncology, Dana Farber Cancer Center, and Departments of Medicine and Genetics, Harvard Medical School, Boston, Massachusetts 02115
[4]Life Sciences Division, Lawrence Berkeley National Laboratory, Berkeley, California 94720
[5]These authors share first authorship.
[6]These authors contributed equally to this work.
[7]Present address: Metabolex, Inc., Hayward, California
[8]Present address: Genentech Inc., South San Francisco, California
[9]Present address: Department of Pathology, University of Vermont Medical School, Burlington, Vermont
[10]Present address: Department of Neurological Surgery, UCSF, San Francisco, California
[11]Present address: N.C.I., SAIC-Frederick, Frederick, Maryland
*Correspondence: dh@biochem.ucsf.edu

Summary

The telomere-stabilizing enzyme telomerase is induced in tumors and functionally associated with unlimited replicative potential. To further explore its necessity, transgenic mice expressing SV40 or HPV16 oncogenes, which elicit carcinomas in pancreas and skin, respectively, were rendered telomerase-deficient. Absence of telomerase had minimal impact on tumorigenesis, even in *terc*$^{-/-}$ generations (G5–7) exhibiting shortened telomeres and phenotypic abnormalities in multiple organs. Analyses of chromosomal aberrations were not indicative of telomere dysfunction or increased genomic instability in tumors. Quantitative image analysis of telomere repeat intensities comparing biopsies of skin hyperplasia, dysplasia, and carcinoma revealed that telomere numbers and relative lengths were maintained during progression, implicating a means for preserving telomere repeats and functionality in the absence of telomerase.

Introduction

Telomeres are nucleoprotein structures at chromosomal ends consisting of short tandem DNA repeats bound by specific proteins that function to maintain chromosomal integrity (Greider, 1996; Blackburn, 2001). Telomeric repeat DNA is synthesized and maintained by telomerase, a specialized reverse transcriptase composed of a catalytic subunit named TERT (telomerase reverse transcriptase) that utilizes an RNA template known as *terc* (telomerase RNA component) (Greider, 1998; Nugent and Lundblad, 1998). Telomerase activity is normally low or undetectable in somatic tissues as well as in primary cells in culture (Kim et al., 1994; Chadeneau et al., 1995). As a result, telomere lengths are reduced with every cell division until a critical short length is reached, eliciting a senescent response (Harley et al., 1990). The short-telomere-mediated entry into replicative senescence appears to require the action of the p53 and Rb tumor suppressor pathways (Counter et al., 1992; Shay et al., 1991; Shay and Wright, 1996). A second telomere-associated proliferation block, termed "crisis," emerges as continued

SIGNIFICANCE

Telomere shortening normally limits the replicative potential of cells, serving as a barrier to carcinogenesis, and activation of telomerase is associated with malignancy in many human cancers. This study examined tumorigenesis in mice where telomerase was absent and telomeres had become shortened and evidently dysfunctional in multiple tissues. Pancreatic islet and epidermal squamous carcinomas developed normally in these mice, despite sterility, atrophy, and other telomere-associated abnormalities in normally proliferative tissues. Thus, when viral oncoproteins commandeer multiple cellular functions, including the Rb and p53 tumor suppressors, tumorigenesis may not be so critically dependent on telomerase. This unexpected tolerance of shortened telomeres and inactive telomerase by developing tumors may prove relevant to strategies aimed at inhibiting telomerase in certain human cancer types.

cell division leads to severe telomere erosion. During crisis, cells suffer genomic instability and death; rare immortalized survivors show restored telomere maintenance and function, most commonly via activation of telomerase activity (Shay et al., 1991; Bodnar et al., 1998; Kiyono et al., 1998; Jiang et al., 1999; Morales et al., 1999). Less commonly, telomere function can be preserved through a telomerase-independent, alternative mechanism of telomere maintenance (ALT) (Bryan et al., 1997; Dunham et al., 2000) that may involve homologous recombination (Lundblad and Blackburn, 1993; McEachern and Blackburn, 1996; Nakamura et al., 1998; Teng and Zakian, 1999, Bechter et al., 2003). In humans, increasing evidence suggests that telomerase upregulation is important for carcinogenesis (Kim et al., 1994; Hahn et al., 1999; Stewart and Weinberg, 2000; Blasco and Hahn, 2003).

Telomerase-deficient mice have been generated via deletion of the mouse *terc* gene encoding the RNA component of telomerase (Blasco et al., 1997). *Terc*$^{-/-}$ mice show phenotypic abnormalities only after successive generations of *terc*$^{-/-}$ intercrosses (Lee et al., 1998; Rudolph et al., 1999). The normality of early generation telomerase null mice is attributed to the relatively long telomeres of laboratory mice, which are 20–50 kb in length, compared with human telomere lengths ranging from 8–15 kb (Kipling, 1997). Telomere shortening in late-generation *terc*$^{-/-}$ mice is associated with a range of histopathological defects in highly proliferative tissues, e.g., germ cell depletion in the testis, uterine and intestinal atrophy, and impaired hematopoiesis.

Several studies have employed *terc*$^{-/-}$ mice to examine the impact of telomere dysfunction on tumorigenesis in vivo. Telomere shortening was shown to modulate tumor phenotypes in a complex manner, correlating with the functional status of the p53 tumor suppressor (Chin et al., 1999; de Lange and DePinho, 1999; Artandi et al., 2000).

We have previously analyzed *terc* expression and telomerase activity in two different transgenic models of multistage tumorigenesis (Blasco et al., 1996). Telomerase activity was upregulated in a majority of islet tumors in RIP1-Tag2 mice, and in high-grade squamous carcinomas in K14-HPV16 mice. Now, to assess the functional importance of telomerase and telomere status in these multistage tumorigenesis pathways, the *terc* gene knockout was established in these lines, and tumor phenotype assessed in successive generations of telomerase null mice, as the constitutional telomere length was progressively shortened to dysfunctional lengths. Remarkably, the data provide evidence that telomerase activity is not essential for either tumorigenesis pathway.

Results

Effects of telomerase loss in late-generation terc$^{-/-}$ RIP1-Tag2 and K14-HPV16 mice

To analyze the contributions of telomerase activity to the tumor biology and malignant progression of pancreatic islet β cells, *terc*$^{-/-}$ SV129 × B6 F1 mice were backcrossed to C57Bl/6J mice, and then crossed to produce generation one (G1) *terc*$^{-/-}$ RIP1-Tag2 mice. G1 *terc*$^{-/-}$ RIP1-Tag2 mice were mated to *terc*$^{-/-}$ mice to produce successive generations of telomerase deficient (G2 through G7) mice, each with shorter constitutional telomeres. Mice at G5–7 developed sterility, leading to reproductive failure and termination of breeding at G7. Prototypical signs of systemic telomere dysfunction (Lee et al., 1998) were

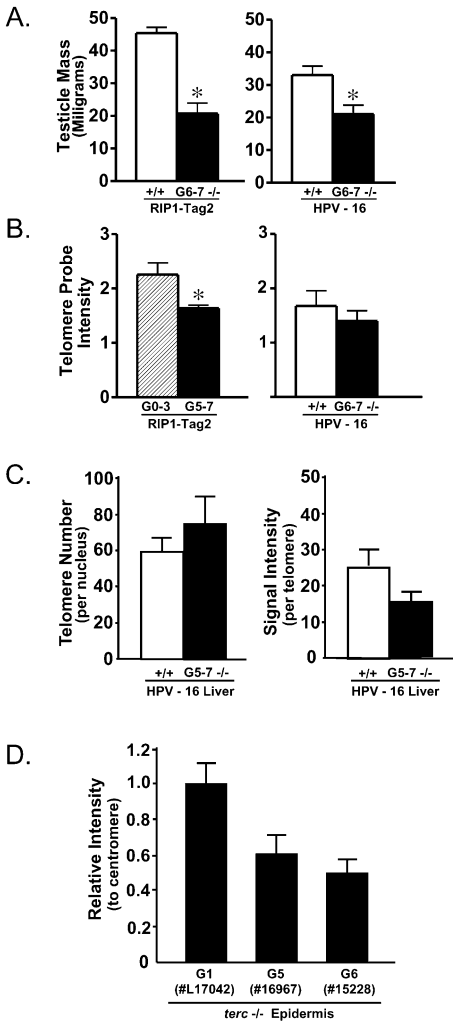

Figure 1. Late generation *terc*$^{-/-}$ RIP1-Tag2 and K14-HPV16 mice evidence telomere shortening and organismic telomere dysfunction

A: A statistically significant decrease in testicular mass was observed for both *terc*$^{-/-}$ RIP1-Tag2 ($p = .0027$) and *terc*$^{-/-}$ HPV-16 ($p = .0067$) mice relative to age-matched RIP1-Tag2 and HPV-16 *Terc*$^{+/+}$ mice (Mann-Whitney t test).

B: Mean telomere content for G0–3 versus G5–7 *terc*$^{-/-}$ RIP1-Tag2 mice and wt versus G6–7 *terc*$^{-/-}$ K14-HPV16 mice was quantified by DNA slot blotting as described in the Experimental Procedures. Tail DNA showed a statistically significant decrease in mean telomere content in G5–7 RIP1-Tag2 *terc*$^{-/-}$ mice ($p = 0.0221$). A reduction in telomere content in tail DNA of G6–7 K14-HPV16 is suggested (although $p = 0.5160$, which is not significant).

C: Quantitative image analysis of images produced by fluorescence in situ hybridization (FISH) using a telomere repeat probe on liver tissue from wt (*terc*$^{+/+}$) and G5–7 *terc*$^{-/-}$ HPV16 transgenic mice showed that telomere numbers were similar if not slightly elevated in the G5–7 liver (left panel), whereas the average hybridization intensity per telomere was reduced (right panel). (For telomere number, $p = 0.01$; for telomere repeat intensity, $p = 0.001$; both by a two-sample t test, assuming equal variances.)

D: Centromere-normalized telomere length in G1, G5, and G6 *terc*$^{-/-}$ mouse epidermis. The telomere hybridization intensity in each tissue section of G5 and G6 *terc*$^{-/-}$ mouse skin was first normalized to its cognate centromere probe, averaged, and then renormalized to the intensity of similarly normalized telomeres in G1 *terc*$^{-/-}$ mouse epidermis. The difference in relative telomere length between G5 and G6 is clearly distinguishable.

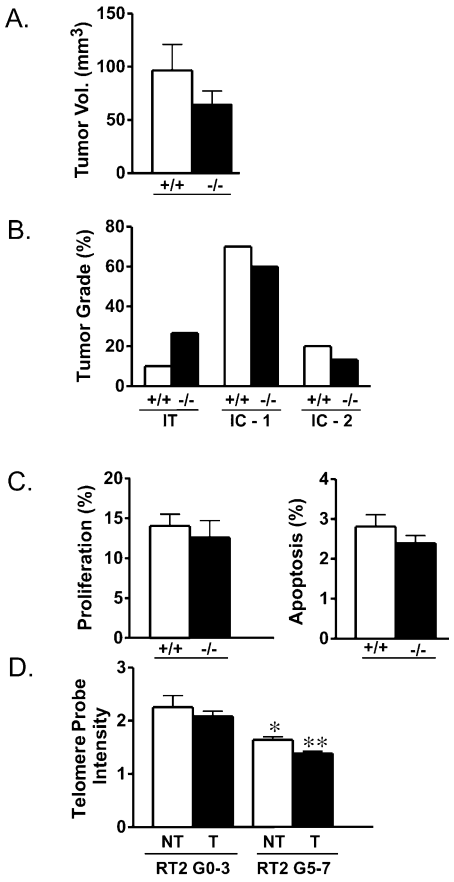

Figure 2. Unaltered pancreatic islet tumor phenotype in G6–7 *terc*$^{-/-}$, RIP1-Tag2 mice

A: Tumor burden was determined in the pancreas of 5 *terc*$^{-/-}$ and 5 wt mice, as described in the Experimental Procedures and methods.

B: The tumors were classified as insulinomas, namely islet tumors with well-defined margins with or without capsules, or as islet carcinomas with focal (type 1) or widespread invasion (type 2). Tumors were graded by histopathology using H&E staining of pancreases from 4 *terc*$^{-/-}$ and 5 wt mice at 13.5 weeks.

C: The proliferation and apoptotic rates were determined in an analysis of tumors in 5 *terc*$^{-/-}$ mice, compared to 5 wt mice.

D: Mean telomere length for G0–3 and G5–7 terc$^{-/-}$ RIP1-Tag2 tumors was quantified by DNA blotting with a telomere probe as described in the Experimental Procedures. Normal tissue (NT), both spleen (shown) and tail (not shown), as well as tumor tissue (T) showed a statistically significant decrease in mean telomere length in G5–7 *terc*$^{-/-}$ mice versus wt terc$^{+/+}$ RIP1-Tag2 mice ($p = 0.0221$ for spleen [NT] tissue comparison; $p<0.0001$ for tumor tissue comparison).

observed in the form of reduced body size and organ atrophy, particularly in the testes (Figure 1A) and spleen (not shown). In addition, consistent with previous observations (Rudolph et al., 1999), G5–7 *terc*$^{-/-}$ mice developed abnormalities of the skin, including hair loss and dermatitis, and slow wound healing, indicating that telomere shortening and presumed dysfunction was impairing skin homeostasis.

K14-HPV16 transgenic mice spontaneously develop squamous carcinomas specifically in the FVB/n background (Coussens et al., 1996). Thus, to assess the contributions of telomerase, *terc*$^{-/-}$ mice were first backcrossed into the FVB/n genetic background for 4 generations, and then mated with K14-HPV16 transgenic mice inbred into FVB/n. *Terc*$^{-/-}$ K14-HPV16 mice were interbred for successive telomerase null generations until sterility terminated the line at G7. The late-generation *terc*$^{-/-}$ K14-HPV16 mice showed organismic hallmarks of telomere dysfunction (Figure 1A and data not shown).

Loss of telomerase function resulted in successive shortening of telomere lengths, reflected in the content of telomeric repeat sequences quantified by slot-blot analysis of genomic DNA using a telomere-specific probe, and by quantitative fluorescence in situ hybridization (Q-FISH) analysis of tissue sections. The slot blot analysis revealed reductions in mean telomere content in normal tissues from both *terc*$^{-/-}$ RIP1-Tag2 and *terc*$^{-/-}$ K14-HPV16 mice (Figure 1B). In situ hybridization to tissue sections of normal liver from wt HPV16 and G5-7 *terc*$^{-/-}$ K14-HPV16 mice using a labeled telomere repeat probe revealed no statistically significant difference in the number of telomeres comparing wt and *terc*$^{-/-}$ liver; there were, however, evident reductions in average telomere length, as ascribed by the hybridization intensity to the telomere repeat probe, when comparing the wt versus G6/7 liver (Figure 1C). To substantiate the sensitivity of the Q-FISH methodology, we performed dual-color Q-FISH using differently labeled centromere and telomere repeat probes, enabling the telomere hybridization intensity to be normalized to that of the centromeres (O'Sullivan et al., 2004). Analysis of three human mammary cell lines of known telomere length demonstrated a good correlation between the centromere-normalized telomere intensity and the actual telomere length, indicating that the method could detect 2 kb differences in average telomere length (Supplemental Figure S1 at http://www.cancercell.org/cgi/content/full/6/4/373/DC1). A similar comparative analysis of the epidermis in skin biopsies of *terc*$^{-/-}$ mice of G1, G5, and G6 (lacking the HPV16 oncogenes) showed a progressive decrease in centromere-normalized telomere length, and further demonstrated that G5 versus G6 lengths were clearly distinguishable (Figure 1D). Thus both DNA blot hybridization and Q-FISH documented that the telomeres were shorter in G5–7 tissues than in wt or G1 tissues, as expected. Further, the Q-FISH analysis showed that similar numbers of telomeres were detected in the G5–7 liver (Figure 1C); this result, as well as the minimal standard error in the centromere normalization of G5/6 epidermis (Figure 1D), indicate that virtually all chromosomes had detectable telomere repeat structures, despite the five to seven generations of telomere shortening effected by the absence of telomerase.

No impact of telomerase deficiency and shortened telomeres on islet carcinogenesis in RIP1-Tag2 mice

We examined multiple parameters of neoplastic progression in G5–7 *terc*$^{-/-}$ RIP1-Tag2 mice. RIP1-Tag2 mice develop pancreatic insulinomas and islet carcinomas, and die of tumor burden and hyperinsulinemia at about 14 weeks of age (Christofori and Hanahan, 1994). There was no apparent change in the tumor phenotype of *terc*$^{-/-}$ RIP1-Tag2 mice from G1 to G4 (not shown). Beginning at G5, when *terc*$^{-/-}$ mice evidence widespread telomere dysfunction (Lee et al., 1998), the tumor phenotype was thoroughly analyzed. Remarkably, there was no significant difference in tumor burden comparing wt RIP1-Tag2 and *terc*$^{-/-}$ RIP1-Tag2 mice near endstage at 13.5 weeks of age (Figure 2A), nor was their brief lifespan affected (not shown). However, a trend toward lower mean tumor volumes can be discerned in late generation *terc*$^{-/-}$ mice (Figure 2A). A similar histological

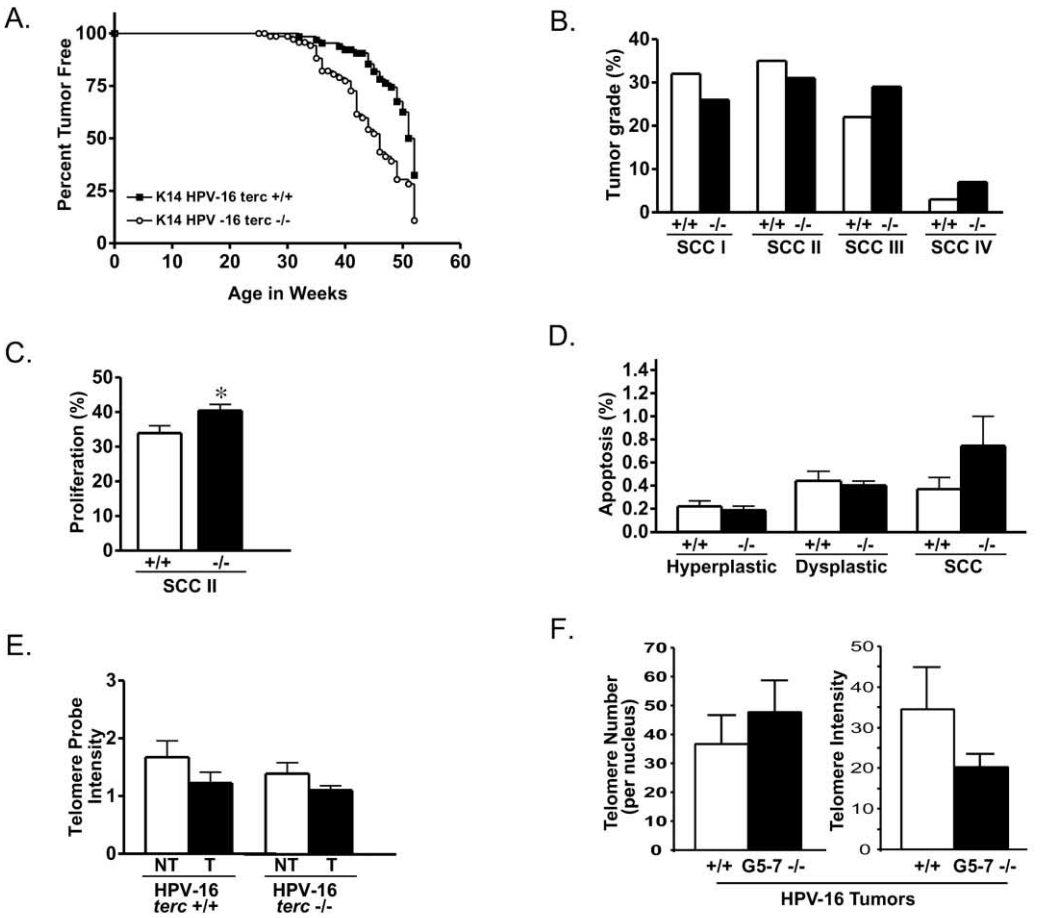

Figure 3. Similar squamous carcinoma phenotype in G6–7 *terc*$^{-/-}$, K14-HPV16 mice

A: The temporal appearance of invasive squamous cell carcinomas of the epidermis in cohort of 76 *terc*$^{-/-}$ HPV16 mice is shown, in comparison to 65 wt HPV16 mice over a 12-month period. By the defined endpoint of 12 months, 50% of the HPV-16 *Terc*$^{+/+}$ mice and 65% of HPV-16 *terc*$^{-/-}$ mice had invasive cancers of varying grades. The earlier onset profile for G6–7 *terc*$^{-/-}$ HPV mice is statistically significant by log rank analysis ($p = 0.0001$).

B: The spectrum of tumor grades ascertained by the progressive loss of squamous differentiated features is shown, revealed by H&E staining of 22 wt and 58 *terc*$^{-/-}$ tumors.

C: The average proliferation index in Grade II squamous cell tumors is shown, in a comparison of 7 wt and 8 *terc*$^{-/-}$ tumors.

D: The apoptotic rates were quantified for hyperplastic and dysplastic lesions, and for tumors from 6 wild-type and 6 *terc*$^{-/-}$ mice. The slight increase in proliferation rate was borderline for statistical significance ($p = 0.037$) by the Mann-Whitney test; otherwise there were no significant differences.

E: Mean telomere content for HPV16 wild-type and *terc*$^{-/-}$ tumors was quantified by DNA blot hybridization. Nontumor (NT) and tumor (T) tissue showed a reduction in mean telomere length, but the differences were not statistically significant.

F: Quantitative telomere-repeat FISH revealed a modest increase in telomere number (consistent with increased ploidy—see Figure 7) in G6–7 *terc*$^{-/-}$ compared to wt tumors (left panel, $p = 0.044$ using a two-sample t test, assuming equal variance) and a clear reduction in average telomere length in

spectrum of tumors (Lopez and Hanahan, 2002) was observed, including "islet tumors" (IT) with well-defined margins and often a fibrous capsule, as well as "islet carcinomas" with focal (class 1; IC-1) or widespread (class 2; IC-2) invasion of exocrine pancreas (Figure 2B). *Terc*$^{-/-}$ RIP1-Tag2 tumors showed similar rates of apoptosis compared to wt RIP1-Tag2 mice, as assayed by TUNEL, while similar levels of proliferation were detected by PCNA staining (Figure 2C).

This similarity of tumor phenotypes led us to investigate the mean telomere lengths in the tumors, since one interpretation of the results would be the maintenance of telomere length by some form of an ALT mechanism. In human cells, the established ALT mechanism, based on homologous recombination to extend telomere lengths, is typically evidenced by relative increases in average telomere repeat content per cell, and by considerable heterogeneity in the telomere intensities seen within a nucleus (Dunham et al., 2000; Henson et al., 2002). In the mouse, this classical ALT telomere pattern has been seen in extensively passaged *terc*$^{-/-}$ transformed fibroblasts (Chang et al., 2003); additionally, apparent telomere length stabilization without such variable extension has been reported in late passage *terc*$^{-/-}$ cell cultures (Hande et al., 1999). We determined mean telomere content by DNA blot hybridization of DNA isolated from pancreatic islet tumor biopsies with a telomere repeat probe. The analysis revealed modest reductions in mean telomere content in *terc*$^{-/-}$ G5–7 islet tumors compared to wt RIP1-Tag2 tumors, as well as in comparison to normal spleen DNA (Figure 2D) and tail DNA (not shown) in the same G5–7 *terc*$^{-/-}$ animals. The data are not diagnostic of the classical ALT-mediated stabilization of telomeres that markedly increases mean telomere lengths.

Consequences of telomere shortening on squamous carcinogenesis in K14-HPV16 mice

K14-HPV16 transgenic mice spontaneously develop epidermal squamous cell carcinomas between 6–12 months, reaching a ~50% incidence at 12 months (Coussens et al., 1996). Multifocal epidermal hyperplasia ensues at 1–2 months, developing into focal, highly proliferative, angiogenic dysplasias from 3–6 months, one of which typically progresses to an invasive carcinoma by 12 months. The other foci of dysplasia in tumor bearing mice, as well as the dysplastic lesions in mice that do not develop cancer by one year, continue in a highly proliferative condition without apparent lesional regression or progression. As such, we anticipated continuing telomere erosion in the absence of telomerase in lesions with a high proliferation index (30%–50% of keratinocytes) over a period of 6–10 months. There was no apparent alteration in tumor phenotype for *terc*$^{-/-}$ K14-HPV16 mice in the early telomerase null generations, much as for the *terc*$^{-/-}$ RIP1-Tag2 mice. Detailed analyses were performed on G5–7 mice, which revealed no impairment of the cancer phenotype, but rather indications of a slightly more aggressive disease. G6 and G7 *terc*$^{-/-}$ K14-HPV16 mice showed a modest but statistically significant shift toward an earlier appearance of epidermal squamous cell cancers (Figure 3A). Application of a grading scheme for squamous cancers based on loss of keratinocyte differentiation markers (Coussens et al., 1996, 2000) revealed that G6-7 *terc*$^{-/-}$ mice had a similar distribution of grade I–IV tumors, with a slight tendency toward higher-grade lesions (Figure 3B). There was also a modest but statistically significant increase in proliferation rates for invasive squamous cell carcinomas of late generation *terc*$^{-/-}$ relative to wt K14-HPV16 mice. A marked increase in the frequency of apoptotic cells was detected in a subset of the G5–7 *terc*$^{-/-}$ invasive carcinomas; by contrast, there was no significant difference in apoptotic rates in precursor lesions (Figure 3D). DNA blotting revealed similar mean telomere repeat content in *Terc*$^{+/+}$ and *terc*$^{-/-}$ tumors, which was modestly reduced compared to normal tissues of the same mouse (Figure 3E). Telomeres were readily detected by telomere repeat FISH, as exemplified in Figure 3G. Quantitative image analysis of telomere repeat hybridization signals within several hundred nuclei per tumor tissue section demonstrated that G5–7 *terc*$^{-/-}$ squamous carcinomas had a modest increase in number of telomeres detected per nucleus in these semi-thin sections (reflecting increased ploidy amongst the tumors analyzed—see below). Much as for the comparison of liver (Figure 1C) and epidermis (Figure 1D) from "normal" *terc*$^{-/-}$ mice (lacking the HPV16 transgene), we saw clear reductions in the average telomere length in G6–7 tumors (Figure 3F). Importantly, the variance in telomere intensities was not markedly different between wt and G6–7 tumors, nor between tumors and liver in the same telomerase null mice (Figure 3E). Both parameters argue against induction of the classical recombination-based ALT pathway, which is characterized by heterogeneously lengthened telomeres (Dunham et al., 2000; Henson et al., 2002; Chang et al., 2003). The minimal effect on skin carcinogenesis is remarkable when considering the 6–10 month period of proliferative hyperplasia and dysplasia that precedes malignant conversion and growth of large protuberant tumors.

No chromosomal instability in telomere-shortened G5–7 RIP1-Tag2 or K14-HPV16 terc$^{-/-}$ tumors

One interpretation of the lack of major effects on tumor phenotype in these two distinctive models is that the tumors are tolerant of genomic disarray and aneuploidy resultant from telomere dysfunction, as a result of the oncogene-induced deficiencies in the p53 and pRb cell cycle checkpoints. An alternative interpretation is that the telomeres are not critically dysfunctional in the hyperproliferative dysplasias and tumors, despite the absence of telomerase and the clear evidence for telomere dysfunction in normal tissues. Notably, evaluation of mean telomere lengths in normal and tumor tissue of G6–7 mice in both models revealed further telomere shortening in tumors relative to the "ground state" length in normal telomerase null tissues (Figures 2D and 3E). Since p53 is abrogated by the viral oncogenes in both models, we predicted, based on observations in *p53*-deficient *terc*$^{-/-}$ mice (Artandi et al., 2000), that

the G6–7 tumors, as inferred by the intensity of telomere repeat hybridization in an analysis of all discrete telomeres in >100 nuclei each of 4 tumors (right panel, p = 0.002 using a two-sample t test, assuming equal variance).

G: Representative images of nuclei in tumor sections analyzed by telomere repeat FISH, comparing a *terc*$^{+/+}$ (left) with a G7 *terc*$^{-/-}$ (right) squamous carcinoma. Both images were obtained with a 63× objective and are shown at the same magnification; the white bar indicates 10 μm.

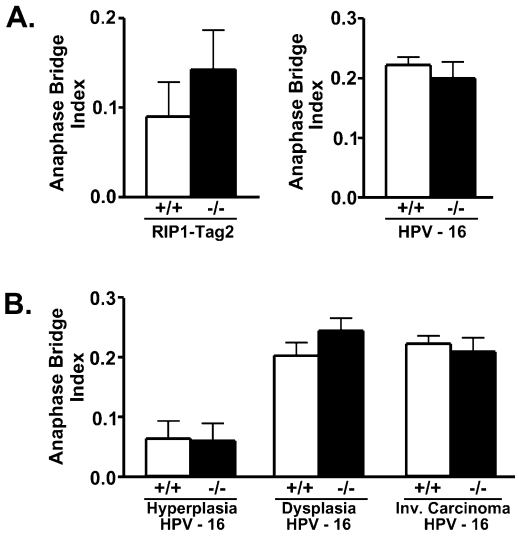

Figure 4. Anaphase bridge analysis is not indicative of increased mitotic dysfunction in late generation telomerase null tumors

The anaphase bridge index in tumors of RIP-Tag2 and HPV16 models was determined as described in the Experimental Procedures, based on comparative analysis of 12 *terc*$^{-/-}$ versus 11 wt *terc*$^{+/+}$ RIP1-Tag2 islet tumors, and of 5 *terc*$^{-/-}$ versus 5 wt *terc*$^{+/+}$ K14-HPV16 tumors. The differences were not statistically significant.

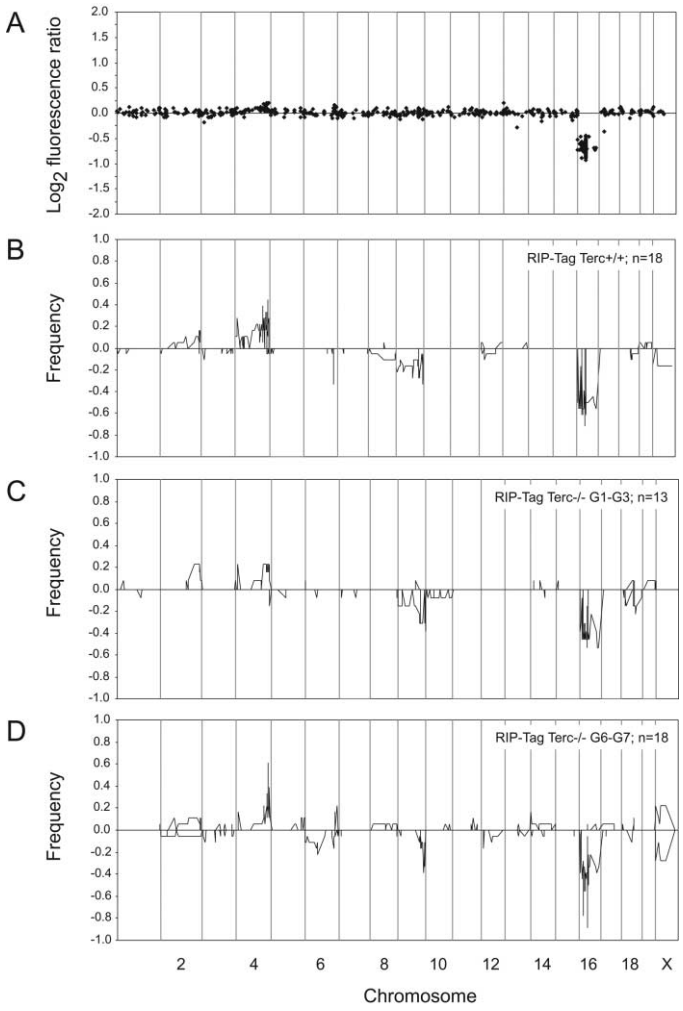

Figure 5. Comparative genomic hybridization analysis of wt versus *terc*$^{-/-}$ pancreatic islet tumors

A: The genome-wide CGH array profile is shown for an islet carcinoma in a G5 *terc*$^{-/-}$ RIP1-Tag2 mouse, which reveals losses on chromosome 16, typical of such tumors in wt RIP1-Tag2 mice (Hodgson et al., 2001). The log (cy3/cy5 fluorescence intensity ratio) of quadruplicate measurements per clone is plotted on the y axis. Clones are arranged along the x axis by chromosome (gray vertical bars delimit the chromosome boundaries); within each chromosome, clones are arranged by their position in the assembled mouse genomic sequence.
B: Frequency of copy number abnormalities (CNA) in wt RIP1-Tag2 tumors.
C: Frequency of CNA in G1–3 *terc*$^{-/-}$ RIP1-Tag2 tumors
D: Frequency of CNA in G6–7 *terc*$^{-/-}$ RIP1-Tag2 tumors.

genomic instability would be induced by critically short telomeres. We addressed this hypothesis in multiple ways. First, we assessed the incidence of anaphase bridges in wt versus G6–7 tumors in each model. Anaphase bridges reflect aberrant chromosomal segregation during mitosis, a marker of telomere dysfunction in yeast (Kirk et al., 1997) and in mouse and human tumors (Rudolph et al., 2001). A slight increase in the anaphase bridge index (ABI) is evident in normal tissues of *terc*$^{-/-}$ relative to wt RIP1-Tag2 mice. There was, however, no significant difference in anaphase bridge frequency comparing wt versus G6–7 islet cell tumors (Figure 4A). Similarly, there was no significant difference in ABI between wt and G6–7 K14-HPV16 mice in either normal skin (not shown) or in squamous carcinomas (Figure 4B). Since the dysplasias in the skin of the K14-HPV16 mice can exist for 6–10 months in a highly proliferative condition without regressing or progressing, we assessed the ABI in a set of hyperplasias and dysplasias from wt and G6–7 *terc*$^{-/-}$ mice; the lesions were collected from mice ranging from 6–12 months of age for both wt and *terc*$^{-/-}$. Again, there was no appreciable difference in ABI between the wt group and the G6–7 *terc*$^{-/-}$ group (Figure 4B). Both *terc*$^{-/-}$ and wt groups evidenced a marked increase in ABI in dysplasia relative to early stage hyperplasia, and both had increased numbers of aberrant mitotic figures and anaphase bridges in carcinomas. Collectively, by the criterion of anaphase bridge frequency, we found no evidence for differential mitotic aberrations in neoplastic lesions of late generation *terc* null mice relative to wt mice, despite concurrent hallmarks of organismic telomere dysfunction.

Next, we sought to assess the degree of genomic alterations as an indicator for the prevalence of genome instability in the telomerase-deficient and control tumors. Given the constraints posed by the sterility and inability to maintain lines of late generation telomerase null RIP1-Tag2 and K14-HPV16 mice, we chose to assess disruptions in the integrity of tumor genomes by profiling genomic copy number abnormalities (CNAs) using array-based comparative genomic hybridization (Hodgson et al., 2001; Pinkel et al., 1998; Pollack et al., 1999). Eighteen G6–7 *terc*$^{-/-}$ RIP1-Tag2 tumors were analyzed, along with 13 tumors from G1–3 *terc*$^{-/-}$ RIP1-Tag2. In line with previous studies, recurrent regional gains and losses were observed, but widespread copy number abnormalities were not detected. Figure 5A shows an array-CGH array profile of one such tumor, revealing a typical loss on mouse chromosome 16. The frequencies of gains and losses across the genome are shown for wt RIP1-Tag2 tumors (Figure 5B), for G1–3 *terc*$^{-/-}$ RIP1-Tag2 tumors (Figure

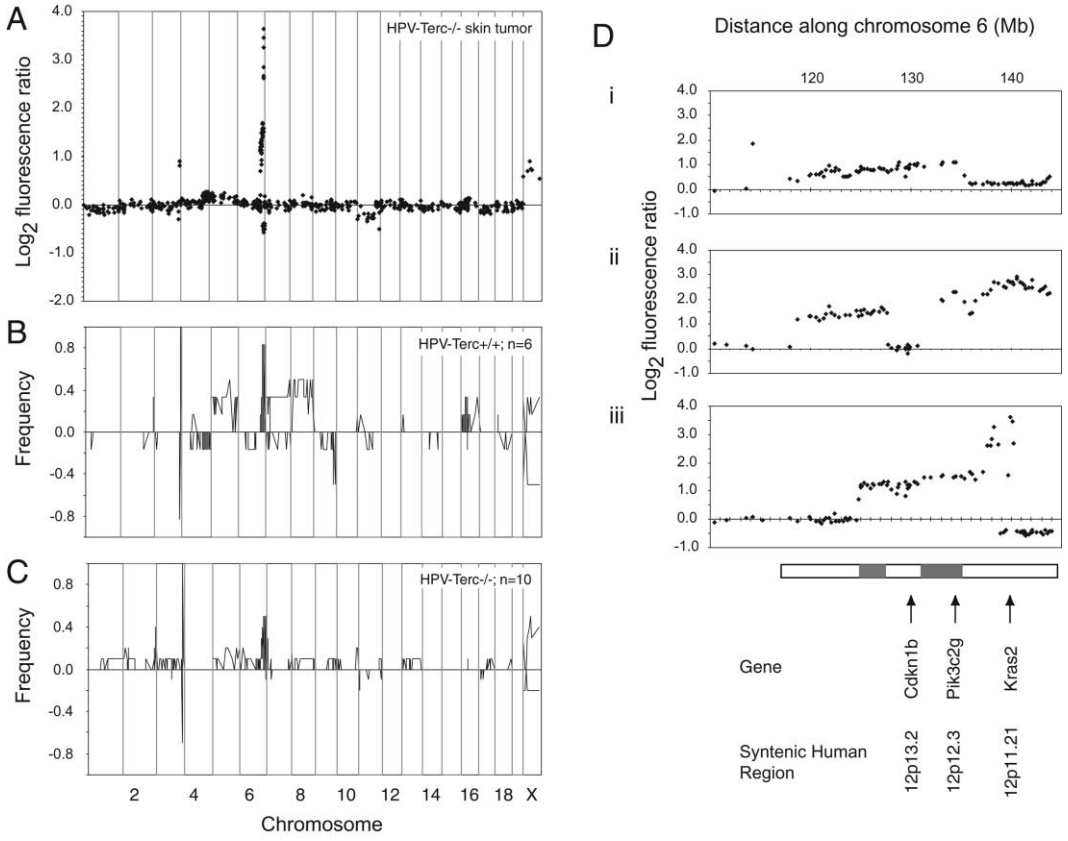

Figure 6. Comparative genomic analysis of wt versus *terc*$^{-/-}$ skin tumors

A: A genome-wide scan of a squamous carcinoma in a G6 *terc*$^{-/-}$ K14-HPV16 mouse. Plot details are given in Figure 5. High-level amplification on chromosome 6 is evident. This region was amplified in 4/10 *terc*$^{-/-}$ tumors, but amplifications were not detected by CGH array analysis of 6 wt tumors. Gain of a small region of chromosome 3 is also apparent; this region was gained in all wt and *terc*$^{-/-}$ K14-HPV tumors examined. The increased fluorescence ratio of the X chromosome clones is reflective of the sex mismatch of the test (tumor) and reference genomes.

B: Frequency of CNA in wt K14-HPV16 tumors.

C: Frequency of CNA in G5–7 *terc*$^{-/-}$ K14-HPV16 tumors.

D: A detailed view of the chromosome 6 amplicon in 3 primary skin tumors (i–iii). Gray bars in the schematic shown at the bottom of the figure indicate regions that are commonly amplified (>2 fold) in all 3 tumors. Genes of interest mapping to this region are shown in addition to their corresponding syntenic human locus. *K-ras2* maps to the region of highest amplification in 2/3 tumors. *Pik3c2G* also maps to the common region. The tumor suppressor *Cdkn1b* (p27) is clearly maintained at normal levels in the tumor shown in ii, despite amplification of proximal and distal sequences.

5C), and for G6–7 *terc*$^{-/-}$ RIP1-Tag2 tumors (Figure 5D); all recurrent CNAs were at loci previously identified in the wt RIP1-Tag2 tumors (Hodgson et al., 2001). The frequency of LOH16 was slightly increased, to ~80% in the G6–7 tumors; by comparison, the frequency of LOH16 in the wt and G0–3 mice ranged from 60%–70%. There was no suggestion of more widespread genomic alterations in these tumors. It is pertinent to recognize that the array CGH technology employed here will only detect copy number changes that are present in more than about 40% of the cells populating a tumor (Hodgson et al., 2001). Nevertheless, array CGH is capable of detecting the rampant aneuploidy characteristic of many human tumors, because clonal selection for particular CNAs likely carries along other random genomic alterations that are not recurrent from tumor to tumor (Pinkel et al., 1998; Pollack et al., 1999). Moreover, analysis of tumors in late generation *terc*$^{-/-}$, *p53*$^{+/-}$ mice previously revealed aneuploidy similar to that observed in human tumors, in the form of end-to-end chromosomal fusions (Artandi et al., 2000); the aneuploidy in those mouse tumors was also detectable in the form of widespread copy number abnormalities using array CGH (O'Hagan et al., 2002). Thus, these viral oncoprotein-driven telomerase-deficient neuroendocrine tumors are not suffering generalized telomere dysfunction and consequent genomic disarray.

We next analyzed 10 skin tumors from G6–7 *terc*$^{-/-}$, K14-HPV16 mice using array CGH, in comparison to 6 tumors from wt K14-HPV16 mice. As for the islet tumors, there was no evidence for widespread disruptions in genomic integrity, consistent with the similar ABI (Figure 4B) comparing G6–7 and wt tumors. A representative tumor profile is shown in Figure 6A. The frequency profile of CNA across the genome is shown for wt K14-HPV16 tumors (Figure 6B) and G6–7 *terc*$^{-/-}$, K14-HPV16 tumors (Figure 6C). Frequent losses (>80%) and gains (100%) were detected in different parts of the distal end of chromosome 3 in both G6–7 *terc*$^{-/-}$ and wt K14-HPV16 tumors. Interestingly, we observed a local amplification (>2 fold) on the distal end of chromosome 6 in 4/10 telomerase null tumors (Figure 6C); two of these were a primary skin tumor and a lymph node metastasis

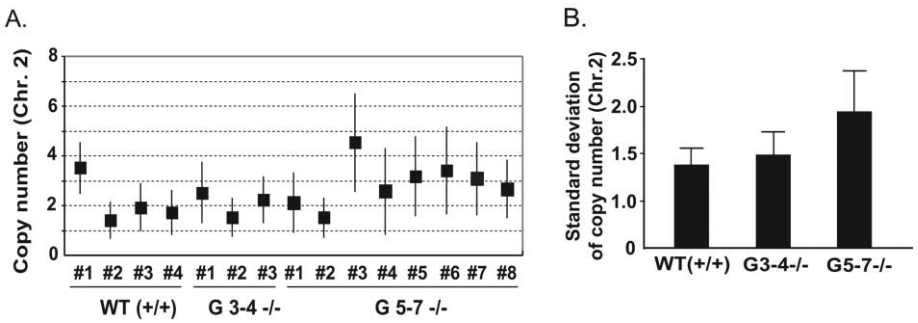

Figure 7. Copy number analysis of a typical chromosome (Chr. 2) detected in semi-thin sections from squamous cell carcinomas in HPV16 mice by FISH

A: The G5–7 tumors are predominantly tetraploid, a conclusion based on the mean copy number of Chr. 2 detected in thin sections, since the analysis involved 4 μ sections that covered about 60% of an intact nucleus. G3–4 tumors were typically diploid or triploid, while wt tumors are generally diploid (an exception is tumor #1, which is tetraploid).

B: Statistical analysis of the variance in chromosome 2 copy number in populations of cells in tumors of the noted *terc* genotypes. Beyond the increase in ploidy, the variance (and the variance of the variance) is not significantly different among the groups. A significant difference would have been indicative of genomic instability in a subset of the cells in a particular population.

from the same animal, and both contained the same amplicon. No such amplification was observed in the 6 wt HPV tumors analyzed herein by array CGH, nor in two independent series of wt tumors analyzed either by traditional CGH to metaphase chromosomes (D. Pinkel and J. Arbeit, personal communication) or by array CGH to microdissected carcinoma cells (L. Coussens et al., personal communication). The copy number increases observed on the distal end of chromosome 6 in wt HPV16 tumors (Figure 6B) consisted of low copy gains. A detailed view of the chromosome 6 amplicon, syntenic with human 12p11-p13, reveals a complex genomic pattern (Figure 6D). *K-ras2* maps to the copy number peak in tumors with the highest level (>8 fold) of amplification, although one tumor did not contain *K-ras2* in its amplicon (Figure 6D). Interestingly, in an analysis of breast, colon, and skin cancers than arose in late generation *terc*$^{-/-}$ *p53*$^{+/-}$ mice, array CGH revealed a high frequency of amplification of this same region on chromosome 6 (O'Hagan et al., 2002).

Since CGH detects recurrent copy number changes in the ensemble of cells in a tumor, it cannot exclude the occurrence of sporadic genomic instability resultant from dysfunctional telomeres in a minor subset of those cells. To address the possibility of episodic instability, we performed FISH analysis of a set of squamous cell carcinomas using a probe to chromosome 2, which shows infrequent abnormalities by array CGH (Figure 6). The rationale was that abnormalities in the number of copies of chromosome 2 per nucleus would be indicative of nonspecific episodic instability in the population of tumor cells; indeed, an analogous experimental design applied to the stages in human breast carcinogenesis revealed just such chromosomal instability (Chin et al., 2004). We evaluated 100 nuclei from wt, G3–4, and G5–7 *terc*$^{-/-}$ HPV16 tumors (n = 3, 4, and 8 each, respectively). From the average numbers of chromosomes 2 signals detected in thin (4 μm) sections representing ~60% of the nucleus, we determined that the wt tumors were with one exception diploid or triploid, as were the G3–4 tumors; the G5–7 tumors were mostly tetraploid (Figure 7A). These differences are reflective of the overall chromosomal ploidy in these tumors (not shown). There was no statistically significant difference in the frequency of nuclei with abnormal numbers of chromosome 2 compared to the mean among the tumors from the three *terc* genotypes (Figure 7B); typically, a few percent of the nuclei in each *terc*$^{-/-}$ genotype had >2× the average copy number of chromosome 2 (i.e., > G2 numbers). The average number of chromosome 2 detected, as well as the variance, and the variance of the variance, were similar (Figure 7B). This analysis does not therefore indicate a differential incidence of episodic instability for chromosome 2, chosen as an unbiased marker chromosome, in the late generation telomerase null tumors that might have been indicative of telomere dysfunction.

Evidence for telomere functionality in G5–7 pancreatic tumors

Further support for the conclusion that the G5–7 tumors largely contain cells with functional telomeres on their chromosomes comes from a study involving serial transplantation of G5–7 islet tumors. Three small tumors (from a G5, a G6, and a G7 *terc*$^{-/-}$, RIP1-Tag2 mouse, respectively) with tumor volumes of 8, 12, and 27 mm^3, were inoculated into immunodeficient (*Rag1* null) mice. In each case, a transplant tumor of >100× volume arose (data not shown). In two cases, ~10 mm^3 pieces of the transplant tumor were serially passaged into new *rag1*$^{-/-}$ mice, and again tumors of 100× volume arose (Table 1). Thus, the G5–7 islet tumors still possessed robust replicative potential.

Telomere stabilization during squamous carcinogenesis

Additional evidence for telomere length maintenance came from comparing relative telomere lengths in the stages of skin carcinogenesis in G6–7 *terc*$^{-/-}$ HPV16 mice. Proliferative hyperplasias develop at 1 month and progress to dysplasias by 3–6 months, which in turn can progress to invasive squamous tumors after persisting in this hyperproliferative condition for up to 9 months. Genetic analyses indicate that dysplasias are progenitors to the tumors and that both are clonal by virtue of containing recurrent chromosomal abnormalities in a majority of cells (L. Coussens, personal communication). Thus, hyperproliferation leading to these tumors lasts 10 months on average and involves at least one clonal selection. The prediction, therefore, is that telomeres should continue to erode during squamous cell carcinogenesis in a G5–7 *terc*$^{-/-}$ HPV16 mouse. To address this expectation, tissue sections of hyperplastic skin, dysplastic skin, and tumor from the same animal were placed side by side on a glass slide, hybridized with a telomere repeat probe, and the hybridizations (exemplified in Figure 3G) captured digitally. The digital images were subjected to quantitative image analysis involving at least 100 nuclei per stage; both the oncogene-expressing hyperproliferative keratinocytes and adjacent stroma (reactive dermis) were evaluated. In addition, we analyzed both epidermal keratinocytes and adjacent dermal

Table 1. Tumor transplantation experiment demonstrating further proliferative capacity of G5-7 terc$^{-/-}$ RIP1-Tag2 tumors

Origin of tumor material transplanted	Size of transplanted tumor	Terc$^{-/-}$ generation	Tumor growth of transplant (dia.)	Notes
RT2, Terc$^{-/-}$ (#92066)	2.5 mm dia. intact tumor	G5	1 cm	First serial passage
RAG1$^{-/-}$ transplant	3 mm^3 fragment		1.2 cm	Serial (2°) passage
RT2, Terc$^{-/-}$ (#"TO1")	3 mm dia. intact tumor	G6	<1 cm	First serial passage
RAG1$^{-/-}$ transplant	3 mm^3 fragment		1.2 cm	Serial (2°) passage
RAG1$^{-/-}$ transplant	3 mm^3 fragment		0.5 cm	Serial (2°) passage
RT2, Terc$^{-/-}$ (#95211)	2 mm dia. intact tumor	G7	0.6 cm	First serial passage
RT2, Terc$^{-/-}$ (#95211)	2 mm dia. intact tumor	G7	0.8 cm	First serial passage

fibroblasts in wt and G5–7 *terc*$^{-/-}$ skin of mice lacking the K14-HPV16 transgene.

We used two methods performed in independent laboratories, one a variation on the method of Lansdorp (Poon and Lansdorp, 2001), and the other an independent algorithm (Ortiz de Solórzano et al., 1999); both are described in the Supplemental Data at http://www.cancercell.org/cgi/content/full/6/4/373/DC1. Each method produced similar results. Four case studies performed on lesional stages from individual mice are shown in Figure 8A. In addition, the average telomere intensities for each stage from the four cases were combined and averaged (see Cases Combined panel); also shown in this panel is a similar determination of the average telomere intensity of keratinocytes in age- and generation-matched *terc*$^{-/-}$ mice lacking the HPV16 oncogenes. Notably, the dermal fibroblasts had greater telomere intensity than the adjacent epidermal keratinocytes in the G5–7 *terc*$^{-/-}$ mice lacking the HPV16 oncogene-induced neoplasia, indicative of greater telomere erosion in the squamous epithelium of the epidermis, wherein progenitor cells (transient amplifying cells) undergo cell division throughout life. Similarly, the keratinocytes in all neoplastic stages had lower telomere intensities than the stromal fibroblasts adjacent to the hyperplasias (cases 1–4, Figure 8A). Surprisingly, the data do not reveal reductions in average telomere length per nucleus in the progression from hyperplasia to dysplasia to clonal tumor. There appears to be a slight reduction in keratinocyte telomere intensity of all neoplastic stages in comparison to normal skin keratinocytes from G5–7 *terc*$^{-/-}$ mice lacking the HPV16 oncogenes (Cases Combined, Figure 8A), but the difference is not statistically significant. We further substantiated this conclusion in a dual-color FISH analysis involving cohybridization with a centromere repeat probe to visualize every chromosome, irrespective of whether it had detectable telomeres. The intensity of each centromere in a nucleus section was determined and combined to give an intensity value, which was then used to normalize the analogous telomere intensity value for that nucleus. A mean normalized telomere value was then established for >200 keratinocytes of a particular stage, with the dysplasias and SCCs further normalized to the value of the hyperplasia, which we infer had had a shorter proliferative lifespan. The analysis of 2 of the cases shown in Figure 8A revealed a modest increase in centromere-normalized telomere intensity in one case, and largely unchanged levels in the other; in neither case was a reduction in telomere intensity evident upon clonal outgrowth of the dysplasias and carcinomas (Figure 8B).

These conclusions rest upon the sensitivity of the Q-FISH methodology employed in our study, and multiple lines of evidence indicate that it is sensitive and quantitative. Dual-label centromere-telomere FISH was used to normalize telomere length (and variance) to the centromeres both in comparisons of (1) three human cell lines of known telomere length (Supplemental Figure S1) and (2) the epidermis in skin biopsies of G1, G5, and G6 terc$^{-/-}$ mice lacking the K14-HPV16 transgene (Figure 1D); in each analysis, Q-FISH detected telomere shortening, consistent with expectations. Furthermore, Q-FISH detected telomere erosion in pairwise comparisons of wt telomerase-proficient versus G5–7 telomerase null normal liver cells (Figure 1C) and wt versus G5–7 tumor cells (Figure 3F).

To address another possibility, that chromosomes with critically shortened telomeres (or lacking telomere-repeats altogether) were present but simply undetectable by our methods, we quantitated the number of telomeres and centromeres per nucleus. If telomeres were becoming lost/undetectable, then the modal telomere number should decline with progression, particularly when normalized to the centromere number. By contrast, the analysis revealed *increasing* numbers of telomeres in the neoplastic keratinocytes, which scaled with the number of centromeres detected in all stages (Figure 8B). We infer that this increase in telomere number correlates with the modal chromosome number, given that the G6–7 tumors were tetraploid, as documented by FISH to chromosome 2 (Figure 7), and that the telomere density per unit nuclear area was constant (Supplemental Figure S2). Thus, there was no indication that telomeres were being lost or shortened below the limits of detection by FISH, in particular during clonal expansion leading to large solid tumors. Moreover, the variance in hybridization intensity per telomere did not increase substantively during progression, even when the telomere length intensity was normalized to that of the centromeres (Figure 8B). We would have expected to see a high variance in average telomere repeat intensity, either per chromosome or per nucleus, if a subset of telomeres were becoming differentially shortened, and/or markedly lengthened (e.g., by the recombination-based ALT mechanism). Rather, there was little change in average telomere intensity or variance in the stages of squamous carcinogenesis in G6–7 *terc*$^{-/-}$ HPV16 mice, either in the single color Q-FISH analysis (Figure 8A) or in the centromere-normalized analysis (Figure 8B).

Discussion

In this study, the necessity of telomerase activity for multistage tumorigenesis has been investigated in two distinctive mouse models, of skin and pancreatic islet carcinogenesis. When the mice were bred successively in the telomerase null background to produce shortened telomeres more analogous to humans, only modest effects were seen on tumor phenotype. There was

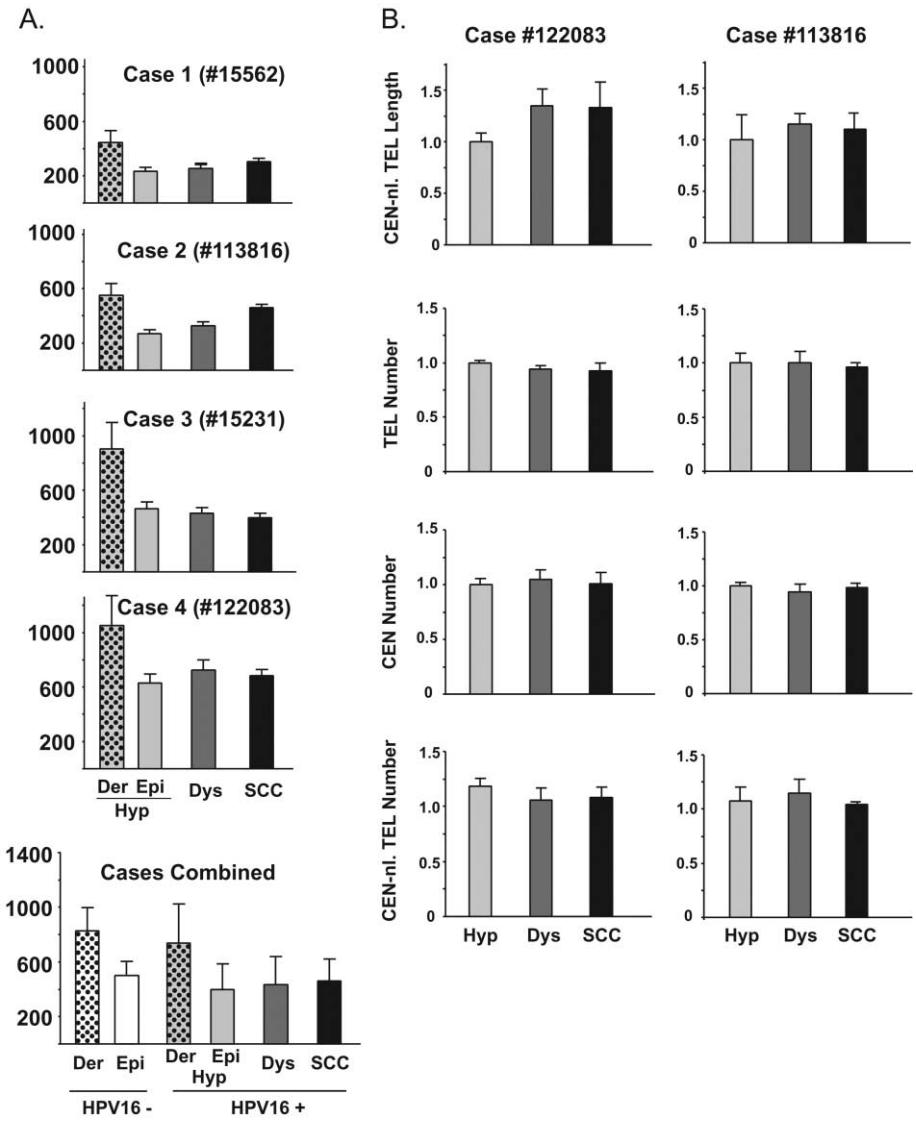

Figure 8. Comparison of telomere intensities in the stages of squamous carcinogenesis of G5–7 HPV16 mice

A: Four case studies are shown, in which tissue sections representing hyperplastic skin (Hyp), dysplastic skin (Dys), and squamous cell carcinoma (SCC) from the same animal were placed on the same microscope slide, hybridized together to a telomere repeat probe, digitally captured in a fluorescence microscope, and analyzed by two independent quantitative image analysis algorithms. Neoplastic epithelial cells (keratinocytes) populating the epidermis or tumors were quantitated, as were the adjacent stromal/dermal fibroblasts in the hyperplasia biopsies. Each method (see the Supplemental Data at http://www.cancercell.org/cgi/content/full/6/4/373/DC1) produced similar results, and those from method 1 are shown, with the y axis indicating the average telomere repeat intensity value per nucleus. The lower panel (Cases Combined) shows the average intensity value of a given stage from the four HPV16 mice, as well as the average intensity from a similar analysis of the keratinocytes in normal skin biopsies (NS) of three similarly aged G5–7 *terc*$^{-/-}$ mice that lack the K14-HPV16 transgene.

B: A dual-color centromere-telomere Q-FISH method (see Experimental Procedures and Supplemental Figure S1) was used to reanalyze two cases (#122083 and #113816) to substantiate the result that telomere lengths were modestly increased in the latter stages of progression, and to assess a possible inability to detect with this Q-FISH method an increasing frequency of chromosomes that lack detectable telomere repeats. The relative intensity of telomere to centromere repeat hybridization per nucleus and then per >200 nuclei was calculated, and the values of dysplasia and cancer were further normalized to the intensity of hyperplasia. In the lower panels, the numbers of telomeres and of centromeres were quantitated and averaged for each stage, and then normalized to the hyperplastic stage. Finally, the average telomere number per stage was normalized to the centromere number, and again to the hyperplastic stage. This analysis indicates that telomere dropout or lack of detectability is not a frequent occurrence in the lesional stages, since if it was, the ratio would drop, and the variance would increase.

no evidence for genomic manifestations of telomere dysfunction in the cells populating neoplastic and malignant lesions in the two models. Collectively, the data support the conclusion that the neoplastic cell populations did not suffer from appreciable telomere dysfunction, despite the absence of telomerase and consequently shortened telomeres that were concomitantly producing aberrations in normal tissues of the same tumor-bearing mice.

Our results stand in provocative contrast to previous studies in other telomerase-deficient cancer-prone mouse strains, which revealed either retarded or substantially altered tumor phenotypes, underscoring the complexity of telomere dynamics and telomerase function in neoplastic initiation and progression (Chin et al., 1999; de Lange and Jacks, 1999). The prior studies in mice can be segmented by the status of the p53 tumor suppressor, which functions as a DNA damage sensor, forcing cells with broken chromosomes into G1 arrest or apoptosis. In gene knockout mice for the tumor suppressors *Ink4a/Arf* or *APC*, where p53 damage-sensing function was intact, late generation *terc*$^{-/-}$ mice had reduced frequencies of cancer and increased survival (Greenberg et al., 1999; Rudolph et al., 2001). Similarly, skin tumorigenesis was reduced in *terc*$^{-/-}$ mice subjected to a classical 2-stage carcinogenesis regimen (Gonzalez-Suarez et al., 2000). On the other hand, in mice where p53 function was directly abrogated by gene disruption, late generation *terc*$^{-/-}$ mice had an altered spectrum of tumors: *p53*$^{+/-}$ and *p53*$^{-/-}$ mice normally develop lymphoid and fibroblastic tumors, whereas late generation *terc*$^{-/-}$ *p53*$^{+/-}$ mice developed frequent epithelial carcinomas concomitant with loss of the wt p53 allele (Artandi et al., 2000). Notably, an indirect measure of telomere

dysfunction, the loss of genomic integrity as assessed by spectral karyotyping (Artandi et al., 2000), array CGH (O'Hagan et al., 2002), or anaphase bridging (Rudolph et al., 2001), indicated that the tumors lacking both telomerase and p53 had chromosomal instability and aneuploidy consistent with critically short, dysfunctional telomeres.

Given that p53 is inactivated by viral oncogenes in both of the models studied here, we expected to see an increase in tumor incidence and/or change in tumor phenotype similar to the results of Artandi et al. (2000). The actuality was a surprising lack of effect: there was no indication of prevalent telomere dysfunction in tumors in either of the models described in this report, dysfunction which should have been revealed either by increases in anaphase bridge frequency, by nonspecific aneuploidy in the form of genome-wide copy number differences detectable by array CGH, and/or by specific aneuploidy of a typical chromosome (Chr 2) analyzed by FISH. Nor was there major alteration in tumor grade or proliferation index. A potentially significant genetic difference between these and the aforementioned models is the direct functional inactivation of both p53 and Rb tumor suppressor proteins, much as occurs in many human tumors; the previous models involved targeting either one or the other suppressor pathway, or both suppressor pathways but at different points (Ink4A/p16 and Arf/p19) that may not be functionally equivalent. Moreover, both the SV40 Tag and the HPV16 E7 oncogenes target suppression of the Rb family at large, inactivating p107 and p130 as well as pRb itself; it is notable that Blasco and colleagues reported involvement of the Rb family in telomere maintenance of telomerase-proficient cells (Garcia-Cao et al., 2002). It must be emphasized, however, that both sets of viral oncogenes used in our models (SV40 large T and small t, or HPV16 E1–E7) co-opt other cellular functions, and one or more of their other targets might prove instrumental in the phenotypes we observe.

Another means for telomere maintenance in tumors?

Our data collectively argue that, despite concurrent dysfunctions in other organs (organ atrophy, small body size, sterility), the telomeres in developing tumors in pancreas and skin induced by these viral oncogenes are somehow maintained in their functionality, and their length. Multiple lines of evidence support this hypothesis: (1) the average telomere intensity, as revealed using two independent quantitative image analysis algorithms of telomere FISH on matched hyperplasias, dysplasias, and squamous carcinomas, was essentially stable, with no evident erosion despite the clonal expansion of the ~1 cm diameter tumors; (2) the number of telomeres per nucleus detectable by telomere-FISH did not decrease, but rather increased congruously with modal chromosome number in neoplasias and tumors; (3) there was no indication of mitotic abnormalities and/or widespread genomic instability in either model; (4) the islet tumors in G5–7 mice could be serially transplanted; and (5) there was little phenotypic impact on either pathway to cancer. While collectively suggesting that the telomeres were somehow maintained in length and functionality, the data do not implicate the classical ALT pathway that produces heterogeneously elongated telomeres, given the stability and low variance in telomere intensity and telomere number revealed by the quantitative (and in some cases centromere-normalized) Q-FISH analysis of the stages in squamous carcinogenesis. In regards to the islet tumorigenesis pathway, technical difficulties with the archival tissue precluded analogous Q-FISH analysis, leaving open the possibility that the ontogeny of islet β cell development and tumorigenesis is tolerant of progressive telomere shortening, in lieu of such a means of telomere stabilization. That said, we favor an alternative explanation, namely that a means of preserving telomere function, an "ALT-2" mechanism, is operative in both of these tumorigenesis pathways. There are at present no clues into the molecular components of this apparent mechanism for maintaining telomere function. One possibility is that ALT-2 involves components of the established recombination-based ALT mechanism, but used in a distinctive way that does not invoke the long and heterogeneous telomere extensions seen in ALT tumors (Cerone et al., 2001). This notion is perhaps consistent with the recent observation that, in certain human cells deficient in telomerase, the ALT capability for preserving telomeres does not invoke generalized activation of homologous recombination but rather acts selectively on telomere repeats (Bechter, et al. 2003).

In conclusion, the data we present clearly implicates a means for preserving telomere length and functionality in tumors expressing viral oncogenes that co-opt multiple cellular functions, including both the Rb and p53 tumor suppressors, but does not reveal the mechanistic components that manifest this capability. It seems likely that this mechanism will be amenable to clarification in genetically engineered cells in culture; the sterility of late-generation *terc*$^{-/-}$ mice and our inability to derive cell lines from the tumors limits the potential for these particular mouse models to serve that purpose. Nevertheless, by carefully analyzing the distinctive stages in tumorigenesis, we have documented a means for preserving telomere function in the absence of telomerase, one that may prove relevant for certain types of human cancer.

Experimental procedures

Anaphase bridge index

An anaphase bridge is defined as the presence of a bridging chromosome over at least 2/3 of the distance between two anaphase poles (Rudolph et al., 2001). These histological structures represent abnormal chromosomal segregation resulting from telomere dysfunction. The anaphase bridge index (ABI) is the ratio of anaphase bridges to the total number of anaphases counted. The ABI was derived from scoring at least 15 anaphases in each tissue of interest in 5 μm paraffin sections stained with hematoxylin and eosin.

Transplantation of G5–7 terc$^{-/-}$ islet tumors into Rag1$^{-/-}$ mice

Small (2 to 3 mm diameter) islet cell tumors were excised from *terc*$^{-/-}$ RIP1-Tag2 pancreatic tissue, washed in sterile PBS at 37°C, and implanted subcutaneously into the flanks of C3HeBFe strain *rag1*$^{-/-}$ mice (Jackson Laboratory). Prior to implantation, *rag1*$^{-/-}$ mice were anesthetized with an I.P. injection of 2.5% Avertin solution, and a small slit on the flank was cut into the skin of the mouse. A pocket under the skin approximately the size of the tumor was enlarged with forceps, and the tumor placed into the pocket. The slit was then sealed closed using cyanoacrylate adhesive (NexaBand, Veterinary Products Laboratories). The implanted mice were observed until the tumor was approximately 1 cm in diameter, or until the deteriorating health of the mouse dictated euthanasia (2–3 months). In either case, the mice were sacrificed and the tumor excised and measured. One transplant tumor arising from a G5 *terc*$^{-/-}$ RIP1-Tag2 primary tumor and another arising from a G6 mouse were each serially passaged by placing a 3 mm^3 fragment of the s.c. transplant tumor tissue subcutaneously into the flank of a C3HeBFe strain *rag1*$^{-/-}$ mouse, as described above; 1 cm tumors again arose several months later.

Supplemental data

For information on transgenic and knockout mice, DNA blot hybridization analysis of genomic DNA for telomere repeat content, histology and immunohistochemistry, array CGH analysis, fluorescence in situ hybridization (FISH) analyses, and quantitative image analysis to evaluate telomere number and average intensity, see the Supplemental Data at http://www.cancercell.org/cgi/content/full/6/4/373/DC1.

Acknowledgments

We thank Michael Rizen for initiating the breeding to establish the *terc*$^{-/-}$ allele in the transgenic mouse backgrounds, Nicole Meyer-Morse for assistance, Monica Miranda for assistance in FISH experiments, Carol Greider for advice and encouragement during the early stages of this project, Titia de Lange and John Murnane for suggestions and encouragement, Kwok-Kin Wong for comments on the manuscript, and Martha Stamper and Paul Yaswen for providing the HMEC lines. This work was supported by grants from the National Cancer Institute.

Received: December 2, 2003
Revised: June 16, 2004
Accepted: August 30, 2004
Published: October 18, 2004

References

Artandi, S.E., Chang, S., Lee, S.L., Alson, S., Gottlieb, G.J., Chin, L., and DePinho, R.A. (2000). Telomere dysfunction promotes non-reciprocal translocations and epithelial cancers in mice. Nature *406*, 641–645.

Bechter, O.E., Zou, Y., Shay, J.W., and Wright, W.E. (2003). Homologous recombination in human telomerase-positive and ALT cells occurs with the same frequency. EMBO Rep. *4*, 1138–1143.

Blackburn, E.H. (2001). Switching and signaling at the telomere. Cell *106*, 661–673.

Blasco, M.A., Rizen, M., Greider, C.W., and Hanahan, D. (1996). Differential regulation of telomerase activity and telomerase RNA during multi-stage tumorigenesis. Nat. Genet. *12*, 200–204.

Blasco, M.A., Lee, H.W., Hande, M.P., Samper, E., Lansdorp, P.M., DePinho, R.A., and Greider, C.W. (1997). Telomere shortening and tumor formation by mouse cells lacking telomerase RNA. Cell *91*, 25–34.

Blasco, M.A., and Hahn, W.C. (2003). Evolving views of telomerase and cancer. Trends Cell Biol. *13*, 289–294.

Bodnar, A.G., Ouellette, M., Frolkis, M., Holt, S.E., Chiu, C.P., Morin, G.B., Harley, C.B., Shay, J.W., Lichtsteiner, S., and Wright, W.E. (1998). Extension of life-span by introduction of telomerase into normal human cells. Science *279*, 349–352.

Bryan, T.M., Englezou, A., Dalla-Pozza, L., Dunham, M.A., and Reddel, R.R. (1997). Evidence for an alternative mechanism for maintaining telomere length in human tumors and tumor-derived cell lines. Nat. Med. *3*, 1271–1274.

Cerone, M.A., Londono-Vallejo, J.A., and Bacchetti, S. (2001). Telomere maintenance by telomerase and by recombination can coexist in human cells. Hum. Mol. Genet. *10*, 1945–1952.

Chadeneau, C., Siegel, P., Harley, C.B., Muller, W.J., and Bacchetti, S. (1995). Telomerase activity in normal and malignant murine tissues. Oncogene *11*, 893–898.

Chang, S., Khoo, C.M., Naylor, M.L., Maser, R.S., and DePinho, R.A. (2003). Telomere-based crisis: Functional differences between telomerase activation and ALT in tumor progression. Genes Dev. *17*, 88–100. Erratum: Genes Dev. *17*, 541.

Chin, L., Artandi, S.E., Shen, Q., Tam, A., Lee, S.L., Gottlieb, G.J., Greider, C.W., and DePinho, R.A. (1999). p53 deficiency rescues the adverse effects of telomere loss and cooperates with telomere dysfunction to accelerate carcinogenesis. Cell *97*, 527–538.

Chin, K., Ortiz de Solorzano, C., Knowles, D., Jones, A., Chou, W., Rodriguez, E.G., Kuo, W.L., Ljung, B.M., Chew, K., Myambo, K., et al. (2004). In situ analyses of genome instability in breast cancer. Nat. Genet. *36*, 984–988.

Christofori, G., and Hanahan, D. (1994). Molecular dissection of multi-stage tumorigenesis in transgenic mice. Semin. Cancer Biol. *5*, 3–12.

Counter, C.M., Avilion, A.A., LeFeuvre, C.E., Stewart, N.G., Greider, C.W., Harley, C.B., and Bacchetti, S. (1992). Telomere shortening associated with chromosome instability is arrested in immortal cells which express telomerase activity. EMBO J. *11*, 1921–1929.

Coussens, L.M., Hanahan, D., and Arbeit, J.M. (1996). Genetic predisposition and parameters of malignant progression in K14–HPV16 transgenic mice. Am. J. Pathol. *149*, 1899–1917.

Coussens, L.M., Tinkle, C.L., Hanahan, D., and Werb, Z. (2000). MMP-9 supplied by bone marrow-derived cells contributes to skin carcinogenesis. Cell *103*, 481–490.

de Lange, T., and DePinho, R.A. (1999). Unlimited mileage from telomerase? Science *283*, 947–949.

de Lange, T., and Jacks, T. (1999). For better or worse? Telomerase inhibition and cancer. Cell *98*, 273–275.

Dunham, M.A., Neumann, A.A., Fasching, C.L., and Reddel, R.R. (2000). Telomere maintenance by recombination in human cells. Nat. Genet. *26*, 447–450.

Garcia-Cao, M., Gonzalo, S., Dean, D., and Blasco, M.A. (2002). A role for the Rb family of proteins in controlling telomere length. Nat. Genet. *32*, 415–419.

Gonzalez-Suarez, E., Samper, E., Flores, J.M., and Blasco, M.A. (2000). Telomerase-deficient mice with short telomeres are resistant to skin tumorigenesis. Nat. Genet. *26*, 114–117.

Greider, C.W. (1996). Telomere length regulation. Annu. Rev. Biochem. *65*, 337–365.

Greider, C.W. (1998). Telomerase activity, cell proliferation, and cancer. Proc. Natl. Acad. Sci. USA *95*, 90–92.

Greenberg, R.A., Chin, L., Femino, A., Lee, K.H., Gottlieb, G.J., Singer, R.H., Greider, C.W., and DePinho, R.A. (1999). Short dysfunctional telomeres impair tumorigenesis in the INK4a(Δ2/3) cancer-prone mouse. Cell *14*, 515–525.

Hahn, W.C., Counter, C.M., Lundberg, A.S., Beijersbergen, R.L., Brooks, M.W., and Weinberg, R.A. (1999). Creation of human tumour cells with defined genetic elements. Nature *400*, 464–468.

Hande, M.P., Samper, E., Lansdorp, P., and Blasco, M.A. (1999). Telomere length dynamics and chromosomal instability in cells derived from telomerase null mice. J. Cell Biol. *144*, 589–601.

Harley, C.B., Futcher, A.B., and Greider, C.W. (1990). Telomeres shorten during ageing of human fibroblasts. Nature *345*, 458–460.

Henson, J.D., Neumann, A.A., Yeager, T.R., and Reddel, R.R. (2002). Alternative lengthening of telomeres in mammalian cells. Oncogene *21*, 598–610.

Hodgson, G., Hager, J.H., Volik, S., Hariono, S., Wernick, M., Moore, D., Nowak, N., Albertson, D.G., Pinkel, D., Collins, C., et al. (2001). Genome scanning with array CGH delineates regional alterations in mouse islet carcinomas. Nat. Genet. *29*, 459–464.

Jiang, X.R., Jimenez, G., Chang, E., Frolkis, M., Kusler, B., Sage, M., Beeche, M., Bodnar, A.G., Wahl, G.M., Tlsty, T.D., and Chiu, C.P. (1999). Telomerase expression in human somatic cells does not induce changes associated with a transformed phenotype. Nat. Genet. *21*, 111–114.

Kim, N.W., Piatyszek, M.A., Prowse, K.R., Harley, C.B., West, M.D., Ho, P.L., Coviello, G.M., Wright, W.E., Weinrich, S.L., and Shay, J.W. (1994). Specific association of human telomerase activity with immortal cells and cancer. Science *266*, 2011–2015.

Kipling, D. (1997). Mammalian telomerase: Catalytic subunit and knockout mice. Hum. Mol. Genet. *6*, 1999–2004.

Kiyono, T., Foster, S.A., Koop, J.I., McDougall, J.K., Galloway, D.A., and Klingelhutz, A.J. (1998). Both Rb/p16INK4a inactivation and telomerase activity are required to immortalize human epithelial cells. Nature *396*, 84–88.

Kirk, K.E., Harmon, B.P., Reichardt, I.K., Sedat, J.W., and Blackburn, E.H. (1997). Block in anaphase chromosome separation caused by a telomerase template mutation. Science *275*, 1478–1481.

Lee, H.W., Blasco, M.A., Gottlieb, G.J., Horner, J.W., 2nd, Greider, C.W., and DePinho, R.A. (1998). Essential role of mouse telomerase in highly proliferative organs. Nature *392*, 569–574.

Lopez, T., and Hanahan, D. (2002). Elevated levels of IGF-1 receptor convey invasive and metastatic capability in a mouse model of pancreatic islet tumorigenesis. Cancer Cell *1*, 339–353.

Lundblad, V., and Blackburn, E.H. (1993). An alternative pathway for yeast telomere maintenance rescues est1$^-$ senescence. Cell *73*, 347–360.

McEachern, M.J., and Blackburn, E.H. (1996). Cap-prevented recombination between terminal telomeric repeat arrays (telomere CPR) maintains telomeres in Kluyveromyces lactis lacking telomerase. Genes Dev. *10*, 1822–1834.

Morales, C.P., Holt, S.E., Ouellette, M., Kaur, K.J., Yan, Y., Wilson, K.S., White, M.A., Wright, W.E., and Shay, J.W. (1999). Absence of cancer-associated changes in human fibroblasts immortalized with telomerase. Nat. Genet. *21*, 115–118.

Nakamura, T.M., Cooper, J.P., and Cech, T.R. (1998). Two modes of survival of fission yeast without telomerase. Science *282*, 493–496.

Nugent, C.I., and Lundblad, V. (1998). The telomerase reverse transcriptase: Components and regulation. Genes Dev. *12*, 1073–1085.

O'Hagan, R.C., Chang, S., Maser, R.S., Mohan, R., Artandi, S.E., Chin, L., and DePinho, R.A. (2002). Telomere dysfunction provokes regional amplification and deletion in cancer genomes. Cancer Cell *2*, 149–155.

Ortiz de Solórzano, C., García Rodriguez, E., Jones, A., Sudar, D., Pinkel, D., Gray, J.W., and Lockett, S.J. (1999). Segmentation of confocal microscope images of cell nuclei in thick tissue sections. J. Microsc. *193*, 212–226.

O'Sullivan, J.N., Finley, J.C., Risques, R.A., Shen, W.T., Gollahon, K.A., Moskovitz, A.H., Gryaznov, S., Harley, C.B., and Rabinovitch, P.S. (2004). Telomere length assessment in tissue sections by quantitative FISH: Image analysis algorithms. Cytometry *58A*, 120–131.

Pinkel, D., Segraves, R., Sudar, D., Clark, S., Poole, I., Kowbel, D., Collins, C., Kuo, W.L., Chen, C., Zhai, Y., et al. (1998). High resolution analysis of DNA copy number variation using comparative genomic hybridization to microarrays. Nat. Genet. *20*, 207–211.

Pollack, J.R., Perou, C.M., Alizadeh, A.A., Eisen, M.B., Pergamenschikov, A., Williams, C.F., Jeffrey, S.S., Botstein, D., and Brown, P.O. (1999). Genome-wide analysis of DNA copy-number changes using cDNA microarrays. Nat. Genet. *23*, 41–46.

Poon, S.S., and Lansdorp, P.M. (2001). Measurements of telomere length on individual chromosomes by image cytometry. Methods Cell Biol. *64*, 69–96.

Rudolph, K.L., Chang, S., Lee, H.W., Blasco, M., Gottlieb, G.J., Greider, C., and DePinho, R.A. (1999). Longevity, stress response, and cancer in aging telomerase-deficient mice. Cell *96*, 701–712.

Rudolph, K.L., Millard, M., Bosenberg, M.W., and DePinho, R.A. (2001). Telomere dysfunction and evolution of intestinal carcinoma in mice and humans. Nat. Genet. *28*, 155–159.

Shay, J.W., Pereira-Smith, O.M., and Wright, W.E. (1991). A role for both RB and p53 in the regulation of human cellular senescence. Exp. Cell Res. *196*, 33–39.

Shay, J.W., and Wright, W.E. (1996). Telomerase activity in human cancer. Curr. Opin. Oncol. *8*, 66–71.

Stewart, S.A., and Weinberg, R.A. (2000). Telomerase and human tumorigenesis. Semin. Cancer Biol. *10*, 399–406.

Teng, S.C., and Zakian, V.A. (1999). Telomere-telomere recombination is an efficient bypass pathway for telomere maintenance in Saccharomyces cerevisiae. Mol. Cell. Biol. *19*, 8083–8093.